
Regression Augmentation With Data-Driven Segmentation

Shayan Alahyari

Department of Computer Science
Western University
London, Ontario, Canada
salahya@uwo.ca

Shiva Mehdipour Ghobadlou

Department of Statistical and Actuarial Sciences
Western University
London, Ontario, Canada
smehdipo@uwo.ca

Mike Domaratzki

Department of Computer Science
Western University
London, Ontario, Canada
mdomarat@uwo.ca

Abstract

Imbalanced regression arises when the target distribution is skewed, causing models to focus on dense regions and struggle with underrepresented (minority) samples. Despite its relevance across many applications, few methods have been designed specifically for this challenge. Existing approaches often rely on fixed, ad hoc thresholds to label samples as rare or common, overlooking the continuous complexity of the joint feature-target space and fail to represent the true underlying rare regions. To address these limitations, we propose a fully data-driven GAN-based augmentation framework that uses Mahalanobis-Gaussian Mixture Modeling (GMM) to automatically identify minority samples and employs deterministic nearest-neighbour matching to enrich sparse regions. Rather than preset thresholds, our method lets the data determine which observations are truly rare. Evaluation on 32 benchmark imbalanced regression datasets demonstrates that our approach consistently outperforms state-of-the-art data augmentation methods.

Keywords: Imbalanced Regression, Augmentation, Oversampling, GAN, Mahalanobis, Distance-based, Geometric

1 Introduction

Imbalanced regression occurs when a continuous target's distribution is skewed, leaving extreme or infrequent values underrepresented and impairing model performance [Krawczyk, 2016]. Standard regressors optimise a global error metric and thus focus on densely sampled regions, neglecting rare values and producing large errors on extremes [Branco et al., 2016, Torgo et al., 2013]. Yet accurate prediction of these infrequent outcomes is vital in many real-world applications [Chawla et al., 2004, Branco et al., 2016, Torgo et al., 2013].

In contrast, imbalanced classification has been studied much more than imbalanced regression. This situation arises when some classes have far fewer examples, causing models to favour majority classes and misdetect minority patterns, yielding high overall accuracy but poor rare-class detection [Guo et al., 2017, Johnson and Khoshgoftaar, 2019]. Domains like fraud detection, medical diagnostics and fault detection depend on recognising these rare classes, so techniques such as oversampling,

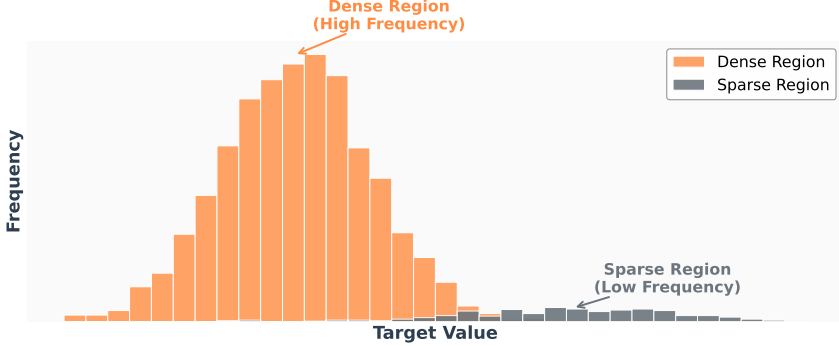


Figure 1: Distribution of target values in an imbalanced regression dataset.

undersampling, cost-sensitive learning and ensemble methods are essential [He and Garcia, 2009, Chawla et al., 2002, Buda et al., 2018, Liu et al., 2009].

Figure 1 demonstrates the distribution of target values in an imbalanced regression dataset. The dense region contains the majority of samples with high frequency, while the sparse region has significantly fewer samples, making it challenging for machine learning models to accurately predict values in the underrepresented areas.

Imbalanced regression impacts many critical real-world applications where accurately predicting rare but high-impact events in the tails of skewed distributions is paramount. For instance, in precision agriculture, vineyard yield datasets feature extreme low- and high-yield blocks that are poorly represented, prompting conditional UNet–ConvLSTM architectures with zonal weighting to address these extremes [Kamangir et al., 2024]. In chemical synthesis planning, high-yield reactions are rarer yet more valuable, yet existing prediction models overlook this imbalance and underperform on critical high-yield bins [Ma et al., 2024]. In meteorology, rare rapid intensification of wind speed is underforecast by deep ConvLSTM models unless reweighted for the right-tail distribution [Scheepens et al., 2023]. In materials engineering, autoencoder-based models with adaptive kernel density weighting correct underrepresentation of extreme steel plate yield strengths [Zhang et al., 2025]. These instances highlight the limitations of traditional regression methods and emphasize the necessity for dedicated imbalanced-regression techniques.

Most oversampling methods impose domain knowledge and ad hoc thresholds to mark rarity, oversimplifying the continuous target structure and often degrading generalization. We propose a fully data-driven pipeline, requiring no arbitrary thresholds, that flags minority points via Mahalanobis distance with Gaussian mixture modelling and then uses a Wasserstein GAN to generate realistic synthetic samples, improving both rare-value accuracy and overall performance. To our knowledge, this is the first approach to combine Mahalanobis-GMM detection with GAN-based generation for imbalanced regression, eliminating the need for manual threshold selection while preserving the statistical properties of minority samples. Our method is specifically designed for tabular data, addressing a critical need in structured data applications.

2 Related work

2.1 Class imbalance

We begin with a brief survey of relevant class imbalance techniques from classification. Chawla et al. [2002] introduced the first data-level class imbalance handling approach, SMOTE, which generated synthetic minority samples $\tilde{\mathbf{x}}$ by interpolating between a minority instance \mathbf{x}_i and one of its k nearest neighbours $\mathbf{x}_{i,\text{nn}}$ according to

$$\tilde{\mathbf{x}} = \mathbf{x}_i + \lambda(\mathbf{x}_{i,\text{nn}} - \mathbf{x}_i), \quad \lambda \sim \mathcal{U}(0, 1).$$

SMOTE became the de facto method for handling class imbalance, spawning many variations. Understanding SMOTE’s interpolation principle is essential as it forms the foundation for regression adaptations like SMOTER and SMOGN that we compare against.

Along with SMOTE and its variations, advanced techniques such as generative adversarial networks (GANs) were extensively explored in the class imbalance literature. Mariani et al. [2018] developed BAGAN, a class-conditional GAN initialized with an autoencoder to produce diverse, high-quality minority images. Tanaka and Aranha [2019] demonstrated that GAN-generated tabular data could replace real samples in classifier training and improve minority recall. Engelmann and Lessmann [2020] designed a conditional WGAN with gradient penalty, auxiliary classifier loss, Gumbel-softmax for categorical features, and cross-layer interactions for mixed-type tables. Sharma et al. [2022] embedded SMOTE-interpolated points into a GAN generator to diversify synthetic minority examples for addressing class imbalance. Jiang et al. [2019] employed an encoder-decoder-encoder GAN on time-series data to detect anomalies via combined reconstruction and adversarial losses. Lee and Park [2021] generated rare-attack intrusion samples with a GAN and retrained a random forest to boost detection.

2.2 Imbalanced regression

Unlike class imbalance, the imbalanced regression problem received relatively little attention. Torgo and Ribeiro [2007] and Torgo et al. [2013] introduced the first data-level method (SMOTER) by extending SMOTE to regression with a relevance function $\phi(y)$ to identify rare targets, undersample common values, and interpolate rare points. Branco et al. [2017] generalized SMOTER by adding Gaussian noise (SMOGN) to increase sample variability, and later proposed WERCS [Branco et al., 2019], which probabilistically oversampled or undersampled based on $\phi(y)$ and simple random or noise generation. Alahyari and Domaratzki [2025a] proposed LDAO, which clusters the joint feature-target space and applies kernel density estimation within each cluster to generate synthetic samples that preserve local distribution characteristics. Camacho et al. [2022] introduced G-SMOTE, incorporating target-space geometry into interpolation, and Camacho and Bacao [2024] replaced hard rarity thresholds with instance-based weighting in WSMOTER. Alahyari and Domaratzki [2025b] developed SMOGAN, a two-stage framework that refines initial synthetic samples through adversarial training with distribution-aware GANs to improve sample quality. Moniz et al. [2018] integrated SMOTE oversampling into boosting (SMOTEBL), demonstrating the adaptability of data-level strategies for regression imbalance.

Alongside data-level strategies, several algorithmic methods were proposed for imbalanced regression. Cost-sensitive learning extended standard regression by weighting errors on rare targets [Zhou and Liu, 2010, Elkan, 2001, Domingos, 1999]. Steininger et al. [2021] introduced DenseLoss, which emphasized low-density targets in the loss function. Yang et al. [2021] applied label-distribution smoothing in deep neural networks. Ren et al. [2022] proposed Balanced MSE to scale error contributions according to target rarity.

There has also been work on developing new evaluation metrics specifically for imbalanced regression problems. Ribeiro and Moniz [2020] developed SERA (Squared Error Relevance Area), a squared-error relevance-weighted metric that addresses the limitations of traditional metrics like RMSE in imbalanced settings. SERA integrates prediction errors across different relevance thresholds, giving more weight to errors on rare target values. This is particularly important because standard regression metrics often mask poor performance on minority samples by being dominated by the abundant majority samples, making specialized metrics like SERA essential for properly evaluating imbalanced regression methods.

2.3 Mahalanobis distance and Gaussian mixture modeling in classification

The Mahalanobis distance measures how far a data point lies from the center of a distribution, accounting for the correlation structure of the data. Unlike Euclidean distance, it takes into account the shape and orientation of the data cloud. This makes it particularly useful for outlier detection and understanding data geometry, which is why we employ it as the foundation of our minority detection approach. We provide formal definitions in Section 3.2.

Recent advances have applied Mahalanobis distance and Gaussian mixture modeling (GMM) in classification. NezhadShokouhi et al. [2020] proposed MAHAKIL, a Mahalanobis-based oversampling method for software defect prediction, demonstrating that Mahalanobis distance can increase intra-class diversity while preserving minority structure. Yao and Lin [2021] introduced EMDO, a Mahalanobis distance-based method that fits multiple ellipsoids using GMM clustering and MOPSO

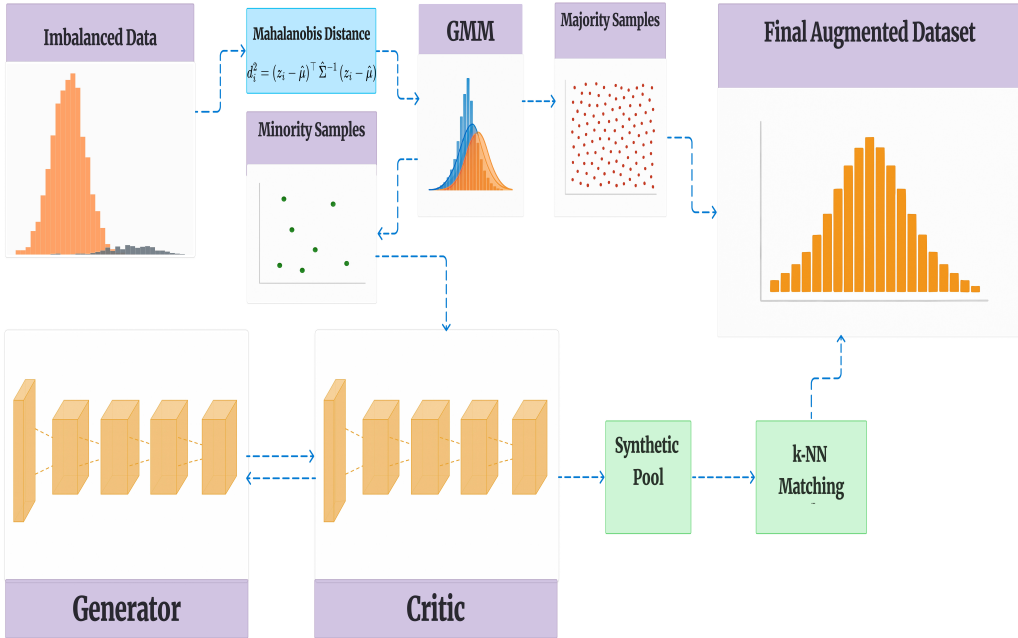


Figure 2: Architecture of the distance-based oversampling approach for imbalanced regression. The framework combines Mahalanobis distance metrics with Gaussian Mixture Models to generate synthetic samples for sparse target regions, using a Generator-Critic mechanism and k-NN matching to ensure synthetic sample quality and dataset balance.

to generate diverse minority samples in multiclass imbalanced settings. In the medical domain, Balakrishnan and Shenoy [2023] developed MMOTE, a Mahalanobis metric-based oversampler that improves minority classification in Parkinson’s disease detection by generating realistic gait samples. For fault diagnosis in electric motors, Ribeiro Junior et al. [2023] combined GMM with Mahalanobis distance to identify mechanical defects, showing high diagnostic accuracy across multiple failure modes.

While these works demonstrate the power of Mahalanobis-GMM methods in classification, their application in imbalanced regression remains unexplored. Our work fills this gap by adapting Mahalanobis-GMM-based detection to the continuous target setting, using it to drive GAN-based synthetic data generation for minority samples.

3 Method

3.1 Overview

Let $\mathbf{x} \in \mathbb{R}^d$ be the feature vector and $y \in \mathbb{R}$ the target; we stack them as $\mathbf{z} = (\mathbf{x}, y) \in \mathbb{R}^p$ with $p = d + 1$. Our procedure comprises three sequential stages: (i) *Mahalanobis-GMM detection*, which fits a univariate Gaussian mixture to the squared Mahalanobis distances of $\{\mathbf{z}_i\}$ and selects the high-distance component as minority samples; (ii) *WGAN-GP generation*, which trains a Wasserstein GAN with gradient penalty on the detected minority set to produce a large synthetic pool; and (iii) *deterministic matching*, which uses a robust Mahalanobis metric to match and filter the synthetic pool, yielding realistic augmentations for downstream regression. Figure 2 illustrates the pipeline of our approach.

3.2 Stage 1: Mahalanobis–GMM minority detection

Let each observation be a joint vector $\mathbf{z} = (\mathbf{x}, y) \in \mathbb{R}^p$, assumed to follow a multivariate Gaussian distribution $\mathbf{z} \sim \mathcal{N}(\boldsymbol{\mu}, \boldsymbol{\Sigma})$, where $\boldsymbol{\mu}$ is the mean vector and $\boldsymbol{\Sigma}$ the $p \times p$ covariance matrix. The

(squared) Mahalanobis distance from \mathbf{z} to the mean is given by [Aggarwal, 2017, Ghorbani, 2019, Ververidis and Kotropoulos, 2008]:

$$d^2(\mathbf{z}) = (\mathbf{z} - \boldsymbol{\mu})^\top \boldsymbol{\Sigma}^{-1} (\mathbf{z} - \boldsymbol{\mu}). \quad (1)$$

In practice, given the training set $\mathcal{D}_{\text{tr}} = \{\mathbf{z}_i\}_{i=1}^n \subset \mathbb{R}^p$, we compute empirical distances using the sample mean and covariance:

$$\hat{\boldsymbol{\mu}} = \frac{1}{n} \sum_{i=1}^n \mathbf{z}_i, \quad \hat{\boldsymbol{\Sigma}} = \frac{1}{n-1} \sum_{i=1}^n (\mathbf{z}_i - \hat{\boldsymbol{\mu}})(\mathbf{z}_i - \hat{\boldsymbol{\mu}})^\top,$$

$$d_i^2 = (\mathbf{z}_i - \hat{\boldsymbol{\mu}})^\top \hat{\boldsymbol{\Sigma}}^{-1} (\mathbf{z}_i - \hat{\boldsymbol{\mu}}), \quad i = 1, \dots, n. \quad (2)$$

Following Goodfellow et al. [2016], Gaussian mixture models are universal approximators of continuous densities. A classical result is that if $\mathbf{z} \sim \mathcal{N}_p(\boldsymbol{\mu}, \boldsymbol{\Sigma})$ then d^2 follows a chi-square distribution with p degrees of freedom [Manly, 2005]. Since the chi-square distribution is heavy-tailed, we model $\{d_i^2\}$ with a two-component GMM, one component capturing the central (majority) bulk, the other capturing the tail (minority). Even if \mathbf{z} is non-Gaussian, this Mahalanobis-GMM combination yields a robust, data-driven heuristic for detecting minority samples in the joint feature-target space.

We fit a two-component Gaussian mixture to the squared distances $\{d_i^2\}$:

$$p(x) = \underbrace{\pi \mathcal{N}(x | \mu_1, \sigma_1^2)}_{\text{minority}} + \underbrace{(1 - \pi) \mathcal{N}(x | \mu_2, \sigma_2^2)}_{\text{majority}} \quad (3)$$

where π is the mixing weight. We estimate the two-component GMM parameters via Maximum Likelihood (ML) using the EM algorithm [McLachlan and Krishnan, 2008]. In practice, EM fitting of two Gaussians flexibly captures the central bulk (μ_1, σ_1^2) and any heavier tails (μ_2, σ_2^2) . The resulting ML cutoff T thus provides a principled, data-driven separator between majority and minority distances by comparing each d_i^2 to T :

$$\begin{cases} d_i^2 < T : & \text{assign to the majority component,} \\ d_i^2 \geq T : & \text{assign to the minority component.} \end{cases}$$

The cutoff T is defined as the unique solution of the weighted-density equality

$$\hat{\pi} \mathcal{N}(T | \hat{\mu}_1, \hat{\sigma}_1^2) = (1 - \hat{\pi}) \mathcal{N}(T | \hat{\mu}_2, \hat{\sigma}_2^2), \quad (4)$$

so that $x = T$ has equal likelihood under both components. After taking logarithms and rearranging, this intersection condition yields the quadratic equation

$$\begin{aligned} & (\hat{\sigma}_1^2 - \hat{\sigma}_2^2) T^2 + (-2\hat{\sigma}_1^2 \hat{\mu}_2 + 2\hat{\sigma}_2^2 \hat{\mu}_1) T \\ & + \hat{\sigma}_1^2 \hat{\mu}_2^2 - \hat{\sigma}_2^2 \hat{\mu}_1^2 - 2\hat{\sigma}_1^2 \hat{\sigma}_2^2 \ln \frac{(1 - \hat{\pi}) \hat{\sigma}_1}{\hat{\pi} \hat{\sigma}_2} = 0, \end{aligned} \quad (5)$$

Solving this quadratic equation provides a fully automatic, statistically principled seed for the subsequent GAN refinement stage.

3.3 Stage 2: Minority sample generation with WGAN-GP

We train a Wasserstein GAN with gradient penalty (WGAN-GP) [Arjovsky et al., 2017, Gulrajani et al., 2017] on the minority set $\mathcal{D}_{\text{min}} \subset \mathbb{R}^p$, defined by the value T from the previous section. We choose WGAN-GP because it provides stable training dynamics and generates diverse, high-quality samples without mode collapse, critical for preserving the complex structure of minority regions in tabular data. Let the generator $G : \mathbb{R}^q \rightarrow \mathbb{R}^p$ and critic $D : \mathbb{R}^p \rightarrow \mathbb{R}$ be multilayer perceptrons with ReLU activations.

Critic loss:

$$\begin{aligned} \mathcal{L}_D = & \mathbb{E}_{\boldsymbol{\epsilon} \sim \mathcal{N}(\mathbf{0}, I_q)} [D(G(\boldsymbol{\epsilon}))] - \mathbb{E}_{\mathbf{z} \in \mathcal{D}_{\text{min}}} [D(\mathbf{z})] \\ & + \lambda_{\text{gp}} \mathbb{E}_{\hat{\mathbf{u}}} \left(\|\nabla_{\hat{\mathbf{u}}} D(\hat{\mathbf{u}})\|_2 - 1 \right)^2, \end{aligned} \quad (6)$$

where $\widehat{\mathbf{u}} = \alpha \mathbf{z} + (1 - \alpha)G(\epsilon)$ with $\alpha \sim \mathcal{U}(0, 1)$.

Generator loss:

$$\mathcal{L}_G = -\mathbb{E}_{\epsilon \sim \mathcal{N}(\mathbf{0}, I_q)} [D(G(\epsilon))]. \quad (7)$$

After convergence, we draw N_{pool} synthetic samples from the generator:

$$\mathcal{D}_{\text{syn}}^{\text{pool}} = \{G(\epsilon_j)\}_{j=1}^{N_{\text{pool}}}, \quad \epsilon_j \sim \mathcal{N}(\mathbf{0}, I_q).$$

3.4 Stage 3: Deterministic Nearest-Neighbour matching

We employ a k-nearest neighbour (k-NN) approach to select high-quality synthetic samples from the generated pool, ensuring they closely match the distribution of real minority points. Let $\mathbf{V} = \hat{\Sigma}^{-1}$ be the precision matrix from Stage 1 (Eq. (1)). While earlier distances were measured from the mean, we now compute pairwise Mahalanobis distances between real and synthetic points. For each real minority point $\mathbf{z}_r \in \mathcal{D}_{\text{min}}$ and each synthetic candidate $\tilde{\mathbf{z}} \in \mathcal{D}_{\text{syn}}^{\text{pool}}$, we compute

$$\delta(\mathbf{z}_r, \tilde{\mathbf{z}}) = \sqrt{(\tilde{\mathbf{z}} - \mathbf{z}_r)^\top \mathbf{V} (\tilde{\mathbf{z}} - \mathbf{z}_r)}. \quad (8)$$

For each \mathbf{z}_r sort the pool by $\delta(\mathbf{z}_r, \cdot)$ and keep the k nearest candidates:

$$\mathcal{N}(\mathbf{z}_r) = \{\tilde{\mathbf{z}}_{(1)}, \dots, \tilde{\mathbf{z}}_{(k)}\},$$

where $\delta(\mathbf{z}_r, \tilde{\mathbf{z}}_{(1)}) \leq \dots \leq \delta(\mathbf{z}_r, \tilde{\mathbf{z}}_{(k)})$.

Next, select the $n_{\text{pick}} \leq k$ closest candidates from $\mathcal{N}(\mathbf{z}_r)$, where n_{pick} is a hyperparameter controlling sample diversity:

$$\mathcal{M}(\mathbf{z}_r) = \{\tilde{\mathbf{z}}_{(1)}, \dots, \tilde{\mathbf{z}}_{(n_{\text{pick}})}\}.$$

We then define the final refined synthetic set as the union over all real minority points:

$$\mathcal{D}_{\text{syn}}^{\text{ref}} = \bigcup_{\mathbf{z}_r \in \mathcal{D}_{\text{min}}} \mathcal{M}(\mathbf{z}_r). \quad (9)$$

3.5 Final augmented dataset

The data presented to the downstream regressor are

$$\mathcal{D}_{\text{train}}^{\text{aug}} = \mathcal{D}_{\text{tr}} \cup \mathcal{D}_{\text{syn}}^{\text{ref}}.$$

This union enriches sparse regions while keeping all original samples intact.

3.6 Hyperparameters and architecture

Our default settings, which can be tuned in practice, are as follows: the generator uses a $q \rightarrow 128 \rightarrow 256 \rightarrow 128 \rightarrow p$ architecture with ReLU activations; the critic uses a $p \rightarrow 256 \rightarrow 256 \rightarrow 128 \rightarrow 1$ architecture with ReLU activations; the latent-noise dimension is $q = 64$; the gradient-penalty coefficient is $\lambda_{\text{gp}} = 10$; the synthetic-pool size is $N_{\text{pool}} = 10,000$; matching first collects the $k = 3$ nearest candidates and then keeps the $n_{\text{pick}} = 1$ closest unused one for each real minority point.

4 Evaluation methodology

We benchmark our framework against current state-of-the-art imbalanced regression oversamplers SMOGN [Branco et al., 2017] and G-SMOTE [Camacho et al., 2022], as well as random oversampling (RO) [He and Garcia, 2009] and a baseline model without any oversampling. We evaluated our method using 32 datasets from the Keel repository [Alcalá-Fdez et al., 2011] and [Branco et al., 2019]. Table 1 shows the number of instances and features for each dataset.

Table 1: Dataset characteristics showing number of instances and features.

dataset	instances	features	dataset	instances	features
a1	198	11	debutanizer	2,394	7
a2	198	11	ele-2	1,056	4
a3	198	11	forestfires	517	12
a7	198	11	fuel	1,764	37
abalone	4,177	8	heat	7,400	11
acceleration	1,732	14	house	22,784	16
airfoilD	1,503	5	kdd	316	18
analcat	450	11	laser	993	4
available_power	1,802	15	maximal_torque	1,802	32
baseball	337	16	meta	528	65
boston	506	13	mortgage	1,049	15
california	20,640	8	sensory	576	11
compactiv	8,192	21	treasury	1,049	15
concrete_strength	1,030	8	triazines	186	60
cpu	8,192	12	wine_quality	1,143	12
lungcancer	442	24	machineCPU	209	6

4.1 Metrics

We compare methods using RMSE, SERA and F_{ϕ_1} :

$$\text{RMSE} = \sqrt{\frac{1}{n} \sum_{i=1}^n (y_i - \hat{y}_i)^2}.$$

SERA [Ribeiro and Moniz, 2020] uses a relevance function $\phi : \mathcal{Y} \rightarrow [0, 1]$, $D^t = \{(x_i, y_i) \mid \phi(y_i) \geq t\}$, $SER_t = \sum_{(x_i, y_i) \in D^t} (\hat{y}_i - y_i)^2$, and

$$\text{SERA} = \int_0^1 SER_t dt$$

Regression precision, recall and F_{ϕ_1} employ threshold t_R and utility $U(\hat{y}_i, y_i) \in [-1, 1]$, where utility $U(\hat{y}_i, y_i)$ quantifies the usefulness of predicting \hat{y}_i when the true value is y_i , based on the relevance of y_i and the error between \hat{y}_i and y_i [Torgo and Ribeiro, 2009, Ribeiro, 2011, Branco et al., 2019]:

$$\begin{aligned} \text{prec}_\phi &= \frac{\sum_{\phi(\hat{y}_i) > t_R} (1 + U(\hat{y}_i, y_i))}{\sum_{\phi(\hat{y}_i) > t_R} (1 + \phi(\hat{y}_i))}, \\ \text{rec}_\phi &= \frac{\sum_{\phi(y_i) > t_R} (1 + U(\hat{y}_i, y_i))}{\sum_{\phi(y_i) > t_R} (1 + \phi(y_i))}, \\ F_{\phi_1} &= \frac{2 \text{prec}_\phi \text{rec}_\phi}{\text{prec}_\phi + \text{rec}_\phi}. \end{aligned}$$

4.2 Experimental framework

We performed 25 random 80/20 train/test splits per dataset, using SERA and RO from ImbalancedLearningRegression [Wu et al., 2022] and SMOGN per [Kunz, 2020]. We trained TabNet [Arik and Pfister, 2021], holding out 20% of training for validation, with Adam (learning rate 1e-4) for

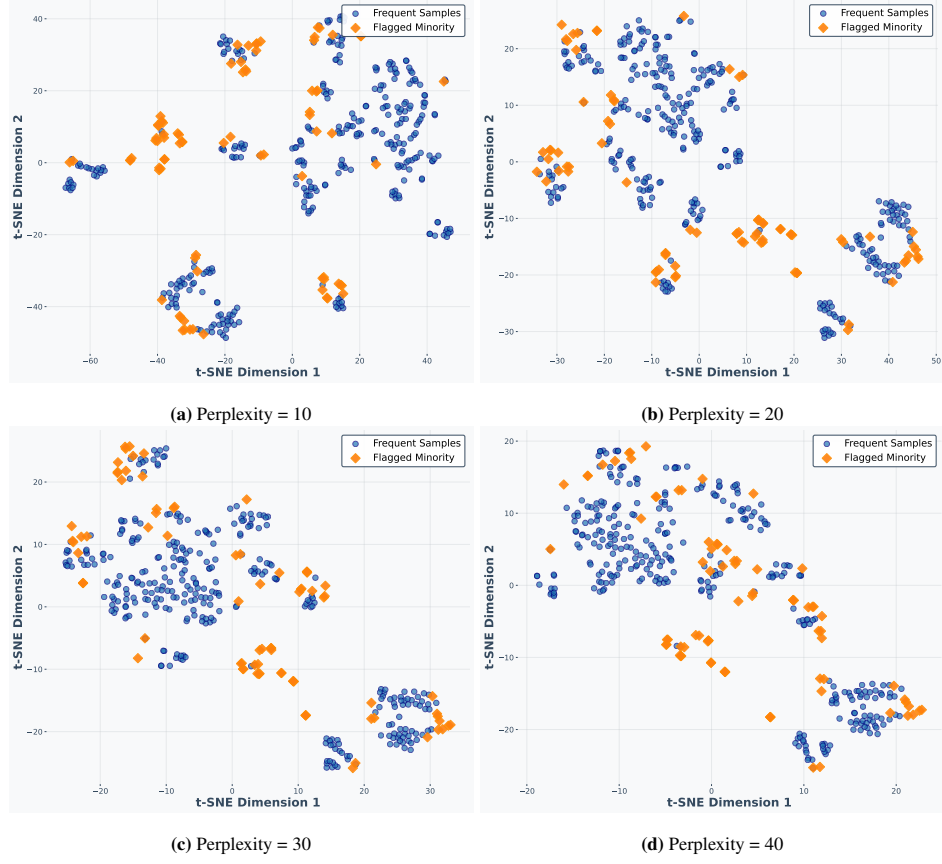


Figure 3: t-SNE visualization with different perplexity values.

up to 1000 epochs, selecting the checkpoint with lowest validation RMSE. Our TabNet comprised six transformer blocks (one initial plus five decision), each containing four 64-unit fully connected layers, five 16-unit attention layers, and one output neuron. We also trained a scikit-learn Random Forest [Breiman, 2001] on the full training set and evaluated it on the test split.

5 Qualitative evaluation

In this section, using the Boston dataset as a representative example, we qualitatively evaluate how our framework captures minority samples in the joint feature-target distribution and assess the quality of the matched nearest neighbours drawn from the synthetic pool generated by our WGAN. The split value determined is $T = 20.13$, which represents the Mahalanobis distance threshold.

5.1 t-distributed stochastic neighbour embedding

t-SNE is a nonlinear dimensionality reduction technique that converts high-dimensional pairwise similarities into probabilities and finds a low-dimensional embedding by minimizing the KL divergence [van der Maaten and Hinton, 2008]. Figure 3 shows Boston dataset embeddings with majority samples as blue circles and minority samples specified by our method as orange diamonds at perplexities 10, 20, 30 and 40. At perplexity 10, local neighbourhoods dominate, fragmenting minority points; at 20, local and global structure balance, forming coherent minority clusters; at 30, small fluctuations are smoothed while preserving cluster separation; at 40, global organisation is most pronounced but fine-grained patterns merge. These results demonstrate that our method reliably captures the true minority structure across both local and global scales.

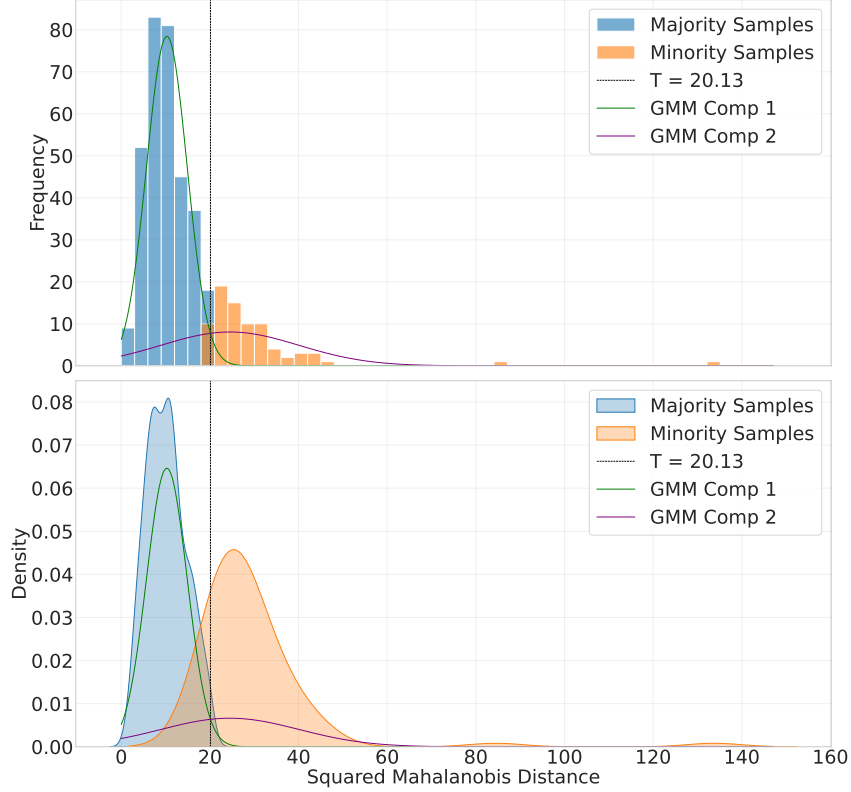


Figure 4: Mahalanobis-GMM analysis on the Boston dataset. Top: frequency histogram of squared Mahalanobis distances for majority (blue) and flagged minority (orange) samples, overlaid with the two GMM component curves (green and purple) and the intersection threshold T . Bottom: corresponding kernel density estimates with the same color scheme and threshold.

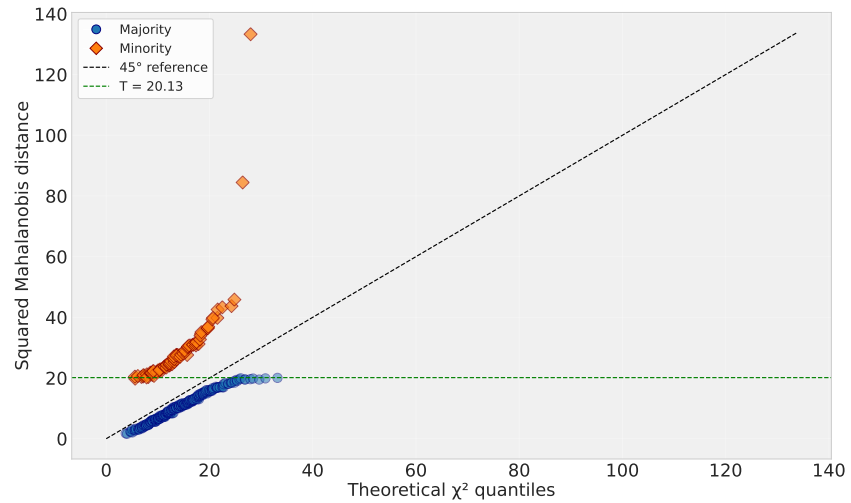


Figure 5: Q-Q plot of squared Mahalanobis distances vs. theoretical χ^2_p quantiles. Blue circles: majority samples; orange diamonds: detected minority samples; black dashed: 45° reference line; green dashed: threshold T .

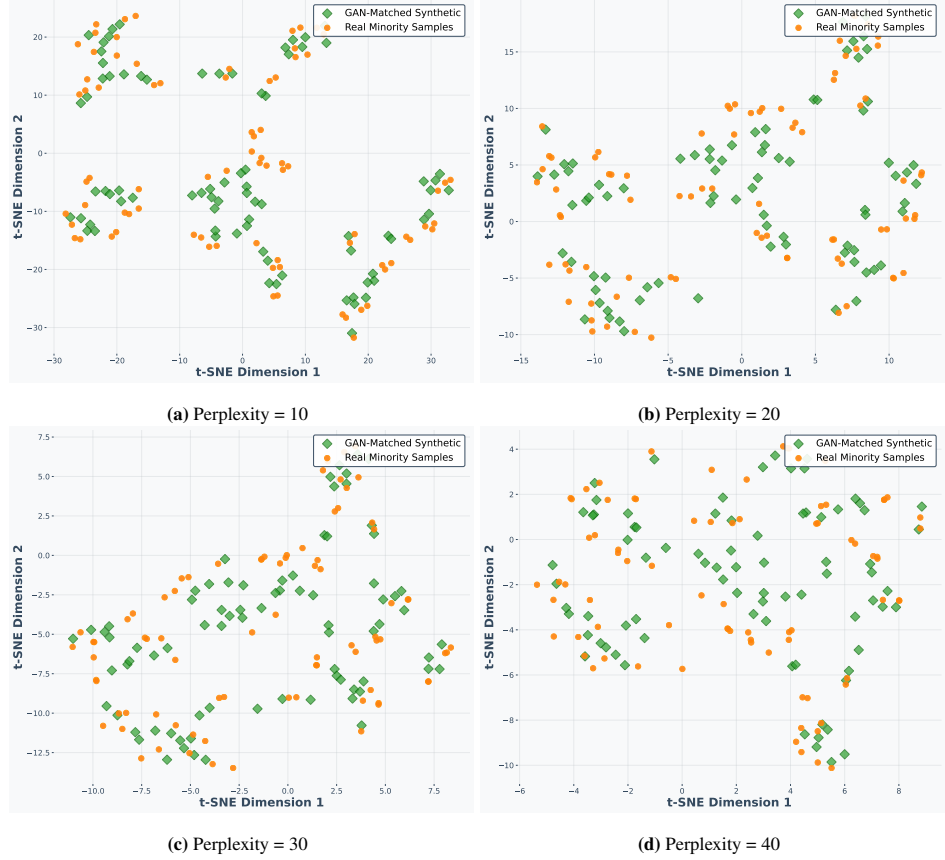


Figure 6: t-SNE embeddings of real minority versus GAN-matched synthetic samples for perplexities of 10, 20, 30, and 40. Real minority samples are orange circles; GAN-matched synthetic samples are green diamonds. Close overlap in each panel confirms that matched synthetic points reproduce the true minority structure across scales.

5.2 Assessment of GMM-based thresholding

The top panel of Figure 4 shows a clear gap in the histogram of squared Mahalanobis distances at the threshold T . The majority samples clusters tightly to the left of T , while the flagged minority samples form a distinct right-hand tail with little overlap. This indicates that the intersection of the two fitted Gaussian components accurately pinpoints the boundary between common and rare observations.

The GMMs defined by Eq. (4) yield two distributions, which we plot in the lower panel of Figure 4. In this panel, the majority density drops sharply to near zero at T , and the minority density increases immediately thereafter. The low-density valley between the two GMM curves aligns perfectly with our cutoff, confirming that the method avoids misclassifying central points as outliers and captures nearly all true extremes. By deriving the threshold directly from the data distribution, without arbitrary thresholds, this procedure adapts to the actual shape of the distance distribution. The result is a robust, automatic selection of genuinely rare samples, providing a reliable input set for the subsequent adversarial refinement stage.

5.3 Chi-square Q-Q analysis of Mahalanobis distances

Figure 5 presents a Q-Q plot comparing the empirical squared Mahalanobis distances to the theoretical χ_p^2 distribution (with p degrees of freedom). Majority samples (blue circles) lie close to the 45° reference line up to the threshold T , confirming that their distances follow the expected χ_p^2 law. In contrast, the flagged minority samples (orange diamonds) systematically exceed T in the upper tail, underscoring their role as genuine outliers. The horizontal green dashed line marks the GMM-

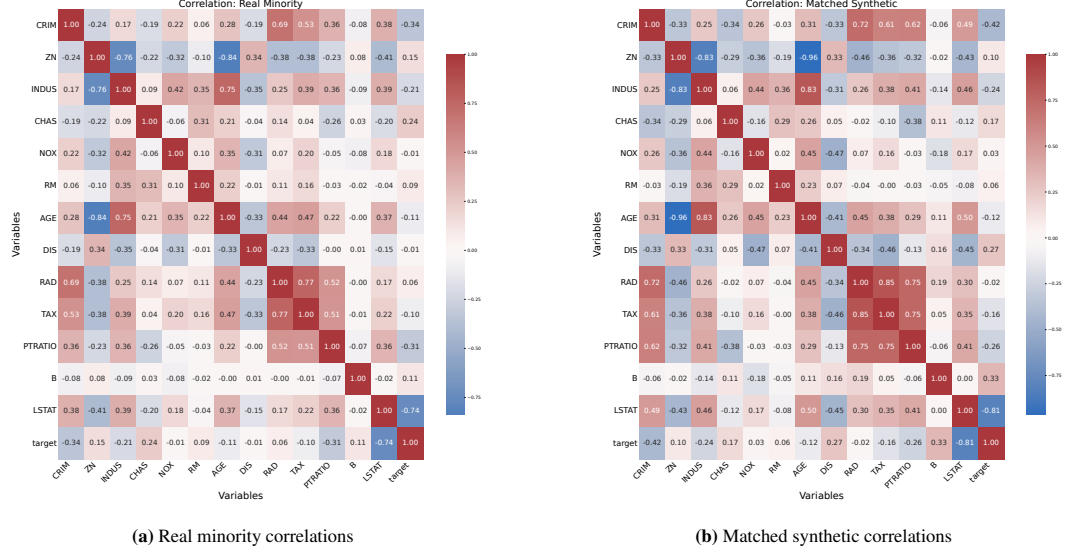


Figure 7: Comparison of feature correlations for real minority versus GAN-matched synthetic samples. Panel (a) shows the Pearson correlation matrix of the real minority data; panel (b) shows the same for matched synthetic data.

derived cutoff T , and deviations of the majority points from the reference line would signal possible misspecification of the covariance estimate.

5.4 t-SNE of real minority vs. matched synthetic samples

We assess the quality of our nearest-neighbour matching by visualizing real minority and GAN-generated samples in a 2D t-SNE embedding on the Boston dataset. Figure 6 shows embeddings at four perplexity settings. Orange circles mark real minority points, and green diamonds mark their matched synthetic counterparts. Across all panels, the synthetic points closely overlap with real clusters, demonstrating that our matching procedure selects synthetic samples which faithfully follow the true minority distribution at both local (low perplexity) and global (high perplexity) scales.

5.5 Correlation structure of real and synthetic minority samples

We compare the pairwise relationships among all 13 features of the Boston dataset (including the target) in the real minority set and in the GAN-matched synthetic set by computing Pearson correlation matrices and visualizing them as heatmaps. Figure 7(a) shows the correlation matrix for the real minority samples, and Figure 7(b) displays the same for the matched synthetic samples, which closely mirror the real correlations. To quantify deviations, Figure 7(c) plots the element-wise difference. Overall, these results demonstrate that our matching procedure preserves the original minority correlation structure across variables.

6 Results

We present the results of comparing our framework with other oversampling methods, including random oversampling (RO), SMOGN, and G-SMOTE, as well as a no-oversampling baseline. In Figures 8 and 9, we report aggregated pairwise comparisons for each evaluation metric (RMSE, SERA, F-measure) for both TabNet and Random Forest models.

For each dataset and each pairwise comparison, a winner is determined based on outcomes across 25 random splits, so each dataset contributes one win per threshold and two wins in total across both thresholds. Specifically, for any two methods under comparison, the method that prevails in the majority of splits is declared the winner. Next, we perform the Wilcoxon signed-rank test for each pairwise comparison. We compute the differences between the 25 split metric values of the two methods to form a difference vector, and then the test assesses whether these differences are

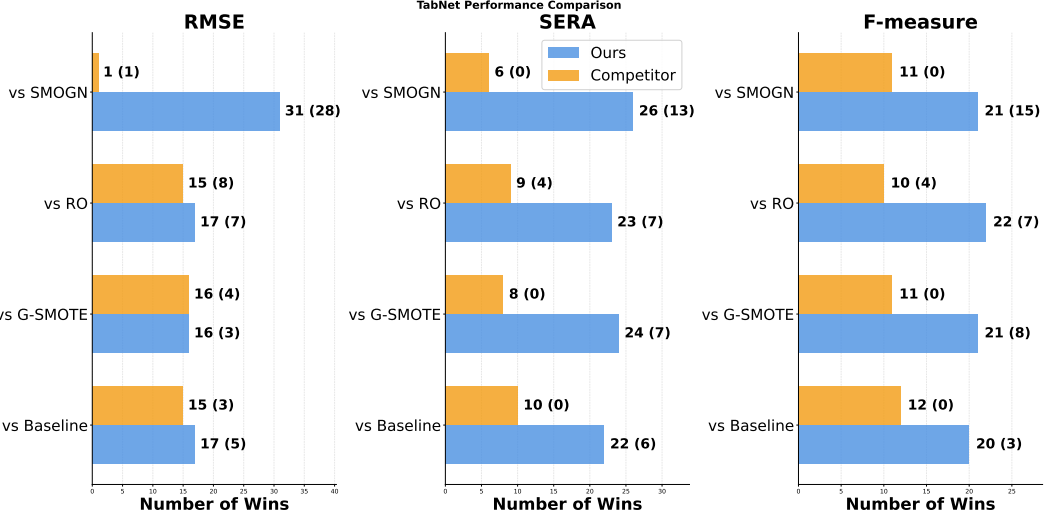


Figure 8: Performance comparison across methods and metrics for TabNet model. Blue bars represent our method’s wins, orange bars represent competitor wins. Numbers show total wins with significant wins in parentheses. Higher values indicate better performance.

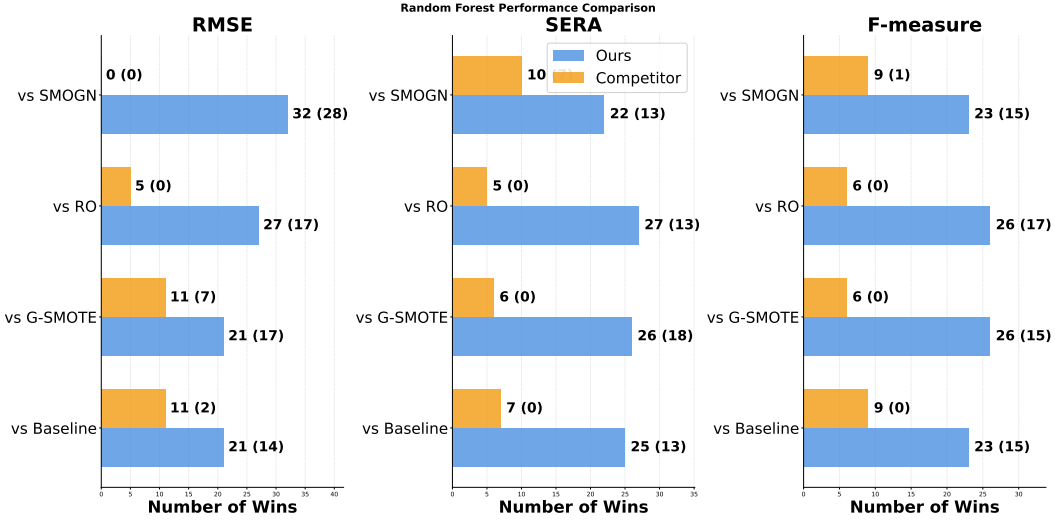


Figure 9: Performance comparison across methods and metrics for random forest model. Blue bars represent our method’s wins, orange bars represent competitor wins. Numbers show total wins with significant wins in parentheses. Higher values indicate better performance.

statistically significant at an alpha level of 0.05, corresponding to a 5% risk of incorrectly concluding that a difference exists when there is none [Wilcoxon, 1945].

In Figures 8 and 9, the numbers outside the parentheses indicate the total number of wins for each method, while the numbers inside the parentheses represent statistically significant wins. Our framework outperforms random oversampling (RO), SMOGN, G-SMOTE and the no-oversampling baseline across all evaluation metrics (RMSE, SERA, F-measure) for both TabNet and Random Forest. It achieves the highest total wins in every pairwise comparison and secures the majority of statistically significant wins, demonstrating that data-driven adversarial and deterministic Mahalanobis matching generate realistic synthetic samples that better align with the true distribution and yield stronger predictive accuracy, even when paired with a powerful regressor like TabNet.

7 Limitations and Discussion

Our approach entails hyperparameter choices that may require tuning. In particular, the nearest-neighbour matching parameters (k and n_{pick}) influence the balance between sample diversity and fidelity, and GAN training introduces computational overhead and sensitivity to network architecture and learning rates. Future work will investigate adaptive strategies for selecting matching parameters, more efficient adversarial training schedules, and extensions to high-dimensional or multimodal regression settings. Overall, our results demonstrate that a data-driven, Mahalanobis-GMM-GAN pipeline can substantially improve rare-target prediction, while offering clear directions for practical refinement.

8 Conclusions

Our framework delivers a fully data-driven pipeline for augmenting imbalanced regression datasets, removing the need for domain expertise or arbitrary rarity thresholds. Comprehensive statistical tests and qualitative visualizations confirm that our Mahalanobis-GMM detection accurately isolates rare observations in the joint feature-target space, and that the WGAN-GP generation followed by deterministic Mahalanobis matching yields realistic synthetic samples that outperform existing oversampling methods (SMOGN, G-SMOTE, and random oversampling) across all evaluation metrics.

References

Charu C Aggarwal. *An introduction to outlier analysis*. Springer, 2017.

Shayan Alahyari and Mike Domaratzki. Local distribution-based adaptive oversampling for imbalanced regression. Preprint arXiv:2504.14316, 2025a.

Shayan Alahyari and Mike Domaratzki. SMOGAN: Synthetic minority oversampling with GAN refinement for imbalanced regression. Preprint arXiv:2504.21152, 2025b.

J. Alcalá-Fdez, A. Fernandez, J. Luengo, J. Derrac, S. García, L. Sánchez, and F. Herrera. Keel data-mining software tool: Data set repository, integration of algorithms and experimental analysis framework. *Journal of Multiple-Valued Logic and Soft Computing*, 17(2-3):255–287, 2011.

Sercan Ö. Arik and Tomas Pfister. Tabnet: Attentive interpretable tabular learning. In *Proceedings of the AAAI Conference on Artificial Intelligence*, volume 35, pages 6679–6687, 2021. doi: 10.1609/aaai.v35i8.16826.

Martin Arjovsky, Soumith Chintala, and Léon Bottou. Wasserstein GAN. *arXiv preprint arXiv:1701.07875v3 [stat.ML]*, 2017.

Kavitha Balakrishnan and Anitha Shenoy. Mmote: A Mahalanobis distance-based oversampling approach for improving minority class classification in parkinson’s disease detection. *Applied Soft Computing*, 136:110174, 2023. doi: 10.1016/j.asoc.2023.110174.

P. Branco, L. Torgo, and R. P. Ribeiro. A survey of predictive modeling under imbalanced distributions. *ACM Computing Surveys*, 49(2):Article 31, 2016.

P. Branco, L. Torgo, and R. P. Ribeiro. SMOGN: A pre-processing approach for imbalanced regression. In *Proceedings of Machine Learning Research: LIDTA*, volume 74, pages 36–50, 2017.

P. Branco, L. Torgo, and R. P. Ribeiro. Pre-processing approaches for imbalanced distributions in regression. *Neurocomputing*, 343:76–99, 2019.

Leo Breiman. Random forests. *Machine Learning*, 45(1):5–32, 2001. doi: 10.1023/A:1010933404324.

M. Buda, A. Maki, and M. A. Mazurowski. A systematic study of the class imbalance problem in convolutional neural networks. *Neural Networks*, 106:249–259, 2018.

L. Camacho and F. Bacao. WSMOTER: A novel approach for imbalanced regression. *Applied Intelligence*, 54:8789–8799, 2024.

L. Camacho, G. Douzas, and F. Bacao. Geometric SMOTE for regression. *Expert Systems with Applications*, 193:116387, 2022.

N. V. Chawla, K. W. Bowyer, L. O. Hall, and W. P. Kegelmeyer. SMOTE: Synthetic minority over-sampling technique. *Journal of Artificial Intelligence Research*, 16:321–357, 2002.

N. V. Chawla, N. Japkowicz, and A. Kolcz. Editorial: Special issue on learning from imbalanced data sets. *ACM SIGKDD Explorations Newsletter*, 6(1):1–6, 2004.

P. Domingos. Metacost: A general method for making classifiers cost-sensitive. In *Proceedings of the 5th ACM SIGKDD International Conference on Knowledge Discovery and Data Mining (KDD)*, pages 155–164, 1999.

C. Elkan. The foundations of cost-sensitive learning. In *Proceedings of the 17th International Joint Conference on Artificial Intelligence (IJCAI)*, pages 973–978, 2001.

Justin Engelmann and Stefan Lessmann. Conditional Wasserstein GAN-based oversampling of tabular data for imbalanced learning. Preprint arXiv:2008.09202v1, 2020.

Hamid Ghorbani. Mahalanobis distance and its application for detecting multivariate outliers. *Facta Universitatis, Series: Mathematics and Informatics*, pages 583–595, 2019.

Ian Goodfellow, Yoshua Bengio, and Aaron Courville. *Deep Learning*. MIT Press, 2016. <http://www.deeplearningbook.org>.

Ishaan Gulrajani, Faruk Ahmed, Martin Arjovsky, Vincent Dumoulin, and Aaron Courville. Improved training of Wasserstein GANs. In *Advances in Neural Information Processing Systems 30 (NeurIPS 2017)*, pages 5767–5777, 2017.

H. Guo, Y. Li, J. Shang, M. Gu, Y. Huang, and B. Gong. Learning from class-imbalanced data: Review of methods and applications. *Expert Systems with Applications*, 73:220–239, 2017.

H. He and E. A. Garcia. Learning from imbalanced data. *IEEE Transactions on Knowledge and Data Engineering*, 21(9):1263–1284, 2009.

Wenqian Jiang, Yang Hong, Beitong Zhou, Xin He, and Cheng Cheng. A GAN-based anomaly detection approach for imbalanced industrial time series. *IEEE Access*, 7:143608–143619, 2019.

J. M. Johnson and T. M. Khoshgoftaar. Survey on deep learning with class imbalance. *Journal of Big Data*, 6(1):1–54, 2019.

Hossein Kamangir, S. Sams, B. Nuno Dokoozlian, Luis Sanchez, and M. Earles, J. Large-scale spatio-temporal yield estimation via deep learning using satellite and management data fusion in vineyards. *Computers and Electronics in Agriculture*, 216:108439, 2024.

B. Krawczyk. Learning from imbalanced data: open challenges and future directions. *Progress in Artificial Intelligence*, 5(4):221–232, 2016.

N. Kunz. Smogn: Synthetic minority over-sampling technique for regression with gaussian noise. PyPI, version v0.1.2, 2020.

JooHwa Lee and KeeHyun Park. Gan-based imbalanced data intrusion detection system. *Personal and Ubiquitous Computing*, 25(1):121–128, 2021.

X.-Y. Liu, J. Wu, and Z.-H. Zhou. Exploratory undersampling for class-imbalance learning. *IEEE Transactions on Systems, Man, and Cybernetics, Part B (Cybernetics)*, 39(2):539–550, 2009.

Yihong Ma, Xiaobao Huang, Bozhao Nan, Nuno Moniz, Xiangliang Zhang, Olaf Wiest, and Nitesh V. Chawla. Are we making much progress? revisiting chemical reaction yield prediction from an imbalanced regression perspective. In *Companion Proceedings of the ACM Web Conference 2024 (WWW '24 Companion)*, pages 791–794. ACM, 2024.

Bryan F. J. Manly. *Multivariate Statistical Methods: A Primer*. Chapman & Hall/CRC Press, Boca Raton, FL ; London, 3rd edition, 2005.

Giovanni Mariani, Florian Scheidegger, Roxana Istrate, Costas Bekas, and Cristiano Malossi. BAGAN: Data augmentation with balancing GAN. Preprint arXiv:1803.09655v2, 2018.

Geoffrey J McLachlan and Thriyambakam Krishnan. *The EM algorithm and extensions*. John Wiley & Sons, 2008.

N. Moniz, L. Torgo, and C. Soares. SMOTEBoost for regression: Improving the prediction of extreme values. In *Proceedings of the 5th International Conference on Data Science and Advanced Analytics (DSAA)*, pages 127–136, 2018.

Mohammad Mahdi NezhadShokouhi, Mohammad Ali Majidi, and Abbas Rasoolzadegan. Software defect prediction using over-sampling and feature extraction based on mahalanobis distance. *The Journal of Supercomputing*, 76(1):602–635, 2020. doi: 10.1007/s11227-019-03051-w.

M. Ren, W. Luo, and R. Urtasun. Balanced mse for imbalanced visual regression. In *Proceedings of the IEEE/CVF Conference on Computer Vision and Pattern Recognition (CVPR)*, pages 418–427, 2022.

R. P. Ribeiro and N. Moniz. Imbalanced regression and extreme value prediction. *Machine Learning*, 109(9-10):1803–1835, 2020.

R. P. A. Ribeiro. *Utility-based regression*. PhD thesis, Faculty of Sciences, University of Porto, Porto, 2011.

Ronny Francis Ribeiro Junior, Fabricio Alves de Almeida, Ariosto Bretanha Jorge, João Luiz Junho Pereira, Matheus Brendon Francisco, and Guilherme Ferreira Gomes. On the use of the Gaussian mixture model and the Mahalanobis distance for fault diagnosis in dynamic components of electric motors. *Journal of the Brazilian Society of Mechanical Sciences and Engineering*, 45:139, 2023. doi: 10.1007/s40430-023-04056-6.

R. Scheepens, D. R. Müller, J. Vos, I. Giannakas, E. Portilla-Figueroa, L. Prieto, and F. Correoso. Adapting a deep convolutional recurrent neural network model for improved spatio-temporal forecasting of extreme wind speed events using imbalanced regression losses. *Geoscientific Model Development*, 16:251–270, 2023.

Anuraganand Sharma, Prabhat Kumar Singh, and Rohitash Chandra. SMOTified-GAN for class imbalanced pattern classification problems. *IEEE Access*, 10:30655–30665, 2022.

M. Steininger, K. Kobs, P. Davidson, A. Krause, and A. Hotho. Density-based weighting for imbalanced regression. *Machine Learning*, 110(8):2187–2210, 2021.

Fabio Henrique Kiyoiti dos Santos Tanaka and Claus Aranha. Data augmentation using GANs. In *Proceedings of Machine Learning Research*, volume XXX, pages 1–16, 2019.

L. Torgo, R. P. Ribeiro, J. P. da Costa, and S. Pal. SMOTE for regression. In *Intelligent Data Engineering and Automated Learning (IDEAL 2013). Lecture Notes in Computer Science*, volume 8206, pages 378–387, 2013.

Luis Torgo and Rita Ribeiro. Utility-based regression. In *Proceedings of the 11th European Conference on Principles and Practice of Knowledge Discovery in Databases (PKDD 2007)*, pages 597–604, 2007.

Luis Torgo and Rita Ribeiro. Precision and recall for regression. In *Discovery Science (DS 2009)*, volume 5808 of *Lecture Notes in Artificial Intelligence*, pages 332–346. Springer-Verlag Berlin Heidelberg, 2009.

Laurens van der Maaten and Geoffrey Hinton. Visualizing data using t-sne. *Journal of Machine Learning Research*, 9:2579–2605, 2008.

Dimitrios Ververidis and Constantine Kotropoulos. Gaussian mixture modeling by exploiting the mahalanobis distance. *IEEE Transactions on Signal Processing*, 56(7):2797–2807, July 2008. doi: 10.1109/TSP.2008.917350.

F. Wilcoxon. Individual comparisons by ranking methods. *Biometrics Bulletin*, 1(6):80–83, 1945.

W. Wu, N. Kunz, and P. Branco. Imbalancedlearningregression-a python package to tackle the imbalanced regression problem. In *Joint European Conference on Machine Learning and Knowledge Discovery in Databases*, pages 645–648, 2022.

J. Yang, L. Xie, Q. Yu, X. He, and J. Liu. Delving into deep imbalanced regression. In *Proceedings of the 38th International Conference on Machine Learning (ICML)*, pages 8437–8447, 2021.

Leehter Yao and Tung-Bin Lin. Evolutionary mahalanobis distance-based oversampling for multi-class imbalanced data classification. *Sensors*, 21(19):6616, 2021. doi: 10.3390/s21196616.

Qian Zhang, Yue Wang, Li Chen, Hao Li, Thanh N. Phan, and Peng Chench. Irmae-akde: A novel deep imbalanced regression approach for performance prediction of rolled steel plate yield strength. *IEEE Transactions on Instrumentation and Measurement*, 74:2006911, 2025.

Z.-H. Zhou and X.-Y. Liu. On multi-class cost-sensitive learning. *Computational Intelligence*, 26(3):232–257, 2010.